Soft Matter

ARTICLE TYPE

Electronic Supplementary information for "Charge regulation mechanism in end-tethered weak polyampholytes"†

D. Prusty,*[a] R.J. Nap ,[b‡], I. Szleifer ,[b‡] and M. Olvera de la Cruz[a]

1 Supporting information for molecular theory

1.1 Density profile expressions and discretization procedure

In this section, we give the expressions for the density of the mobile species and the Poisson equation. The minimization of the free energy functional W, Eqn 12 in the main text, with respect to the density profiles of water and ions yields

$$\phi_w(\mathbf{r}) = \exp(-\beta\pi(\mathbf{r})v_w), \tag{1}$$

$$\phi_{Na^+}(\mathbf{r}) = \frac{v_{Na^+}}{v_w}\exp(-\beta\pi(\mathbf{r})v_{Na^+})\exp(-\beta e\psi(\mathbf{r}))\exp(\beta\mu_{Na^+}), \tag{2}$$

$$\phi_{Cl^-}(\mathbf{r}) = \frac{v_{Cl^-}}{v_w}\exp(-\beta\pi(\mathbf{r})v_{Cl^-})\exp(\beta e\psi(\mathbf{r}))\exp(\beta\mu_{Cl^-}), \tag{3}$$

$$\phi_{H^+}(\mathbf{r}) = \frac{v_{H^+}}{v_w}\exp(-\beta\pi(\mathbf{r})v_{H^+})\exp(-\beta e\psi(\mathbf{r}))\exp(\beta(\mu_{H^+}-\mu^o_{H^+})), \tag{4}$$

$$\phi_{OH^-}(\mathbf{r}) = \frac{v_{OH^-}}{v_w}\exp(-\beta\pi(\mathbf{r})v_{OH^-})\exp(\beta e\psi(\mathbf{r}))\exp(\beta(\mu_{OH^-}-\mu^o_{OH^-})). \tag{5}$$

The chemical potentials are determined by the bulk concentration of all species, namely,

$$\phi_w^{bulk} = \exp(-\beta\pi^{bulk}v_w), \tag{6}$$

$$\phi_{Na^+}^{bulk} = \frac{v_{Na^+}}{v_w}(\phi_w^{bulk})^{\frac{v_{Na^+}}{v_w}}\exp(\beta\mu_{Na^+}), \tag{7}$$

$$\phi_{Cl^-}^{bulk} = \frac{v_{Cl^-}}{v_w}(\phi_w^{bulk})^{\frac{v_{Cl^-}}{v_w}}\exp(\beta\mu_{Cl^-}), \tag{8}$$

$$\phi_{H^+}^{bulk} = \frac{v_{H^+}}{v_w}(\phi_w^{bulk})^{\frac{v_{H^+}}{v_w}}\exp(\beta(\mu_{H^+}-\mu_{H^+})), \tag{9}$$

$$\phi_{OH^-}^{bulk} = \frac{v_{OH^-}}{v_w}(\phi_w^{bulk})^{\frac{v_{OH^-}}{v_w}}\exp(\beta(\mu_{OH^-}-\mu_{OH^-})), \tag{10}$$

The bulk reference solution is assumed be charge neutral and incompressible. The salt is assumed to be completely dissociated and the pH is adjusted by adding either HCl or NaOH depending on the desired value of pH[1]. Please note that ψ^{bulk} is constant and hence, has been set to zero.

Finally, the variation of the free energy functional W with respect to $\psi(\mathbf{r})$ results Poisson equation and its boundary conditions

$$\varepsilon_r\varepsilon_o\nabla^2\psi + \langle\rho_q(\mathbf{r})\rangle = 0 \tag{11}$$

The boundary condition are

$$\frac{\partial\psi(\mathbf{r})}{\partial z}|_{z=0} = 0 \tag{12}$$

and

$$\psi(\mathbf{r})|_{\text{bulk}} = 0 \tag{13}$$

The incompressibility constraint and the Poisson Equation need to be solved simultaneously. Note that its unknowns are the Lagrange multipliers or lateral pressures, $\pi(r)$, the electrostatic potential, $\psi(r)$ and under poor solvent conditions, the density of the polymer as well, $\langle\rho_A(r)\rangle$ and $\langle\rho_B(r)\rangle$ Solutions can be obtained by substituting the expressions of the volume fractions of all components into the incompressibility constraint and the Poisson equation. This results in a set of non-linear integrodifferential equations. By discretizing the space, these equation can be converted into a set of coupled non-linear algebraic equations, which then can be solved numerically[2]. For detailed discretized expressions, the reader is referred to the previous publications[1,3]. The required inputs are the bulk pH, acid dissociation constants of monomers, bulk salt concentration, the grafting density (for 1D calculations) or the grafting pattern (for 3D calculations), a set of polymer conformations. and the volumes of all the mobile species. For three dimensional calculations, periodic boundary conditions in x and y directions were imposed and a hexagonal lattice for the placement of grafting sites was employed. In this coordinate system, the horizontal axes, u and v, are at 60^o to each other. The mapping between x,y,z coordinate system and u,v,z coordinate system follows the following relations:

$$v = \frac{x\cos(\pi/12) - y\sin(\pi/12)}{\sqrt{\cos^2(\pi/12) - \sin^2(\pi/12)}}, \tag{14}$$

$$u = -\frac{x\sin(\pi/12) + y\cos(\pi/12)}{\sqrt{\cos^2(\pi/12) - \sin^2(\pi/12)}}, \tag{15}$$

$$z = z, \tag{16}$$

[a] Department of Materials Science and Engineering, Northwestern University, Evanston, Illinois 60208, United States
[b] Department of Biomedical Engineering, Northwestern University, Evanston, Illinois 60208, United States
[c] Chemistry of Life Processes Institute, Northwestern University, Evanston, Illinois 60208, United States
[d] Department of Chemistry, Northwestern University, Evanston, Illinois 60208, United States
[e] Department of Physics and Astronomy, Northwestern University, Evanston, Illinois 60208, United States

Here, we only give the discretized version of the Van der Waals term in equation 13. The function $g(|\mathbf{r}-\mathbf{r'}|)$ is $(\ell/|r-r'|)^6$ and confined to the range $\ell < |\mathbf{r}-\mathbf{r'}| < 1.5\delta$. Hence, the discrete version of PDFs read:

$$
\begin{aligned}
P(\alpha,j) = &\frac{1}{q_j}\exp(-\sum_{a=A,B}\sum_{b=A,B}\sum_{k,l,m}\sum_{k',l',m'}\beta\varepsilon_{ab}\, g(k-k',l-l',m-m') \\
&n_a(\alpha,j,k,l,m)\langle\phi_b(k',l',m')\rangle \\
&\times\exp(-\beta\sum_{k,l,m}\pi(k,l,m)[v_A n_A(\alpha,j,k,l,m)+v_B n_B(\alpha,j,k,l,m)]) \\
&\times\exp(-\sum_{k,l,m} n_A^{dis}(\alpha,j,k,l,m)(\ln f_{A^-}(k,l,m)-\beta e\psi(k,l,m)) \\
&\times\exp(-\sum_{k,l,m} n_B^{dis}(\alpha,j,k,l,m)(\ln f_{BH^+}(k,l,m)+\beta e\psi(k,l,m)),
\end{aligned}
\tag{17}
$$

Here, $n_a(\alpha,j,k,l,m)$ is the number of monomers of type a belonging to αth conformation of jth graft located in the cell with the index k, l and m. $g(k-k',l-l',m-m')$ is the discretized version of $g(|\mathbf{r}-\mathbf{r'}|)$ and is obtained by integration of the vdW attractions in the cells of the hexagonal lattice by using a Monte Carlo procedure according to the following expression:

$$
\begin{aligned}
&g(k-k',l-l',m-m') \\
&\quad=\int_{\delta(k-k'-\frac{1}{2})}^{\delta(k-k'+\frac{1}{2})}\int_{\delta(l-l'-\frac{1}{2})}^{\delta(l-l'+\frac{1}{2})}\int_{\delta(m-m'-\frac{1}{2})}^{\delta(m-m'+\frac{1}{2})}(\ell/|r-r'|)^6 dvdudz,
\end{aligned}
\tag{18}
$$

where ℓ is the segment length of monomers.

In order to ensure that the obtained profiles indeed represent the minimized solutions, we compute the free energy of the system through two expressions. The first one is the original expression (Eqn. 12 in the main text) and the value of free energy is obtained by numerically substituting the obtained density profiles into this expression. The second expression is obtained by substituting the expressions for density profiles (Eqns. 1 through 5), dissociation profiles (Eqns. 14 and 15 in the main text) and the chain conformation probabilities (Eqn. 13 in the main text), obtained from the minimization of free energy, into the original free energy expression. The resulting expression does not contain any probability terms and depends only the density profiles, the electrostatic potential, the Lagrange multiplier field and the polymer normalization constants (q_j). For the 3D case, it is given by

$$
\begin{aligned}
\beta W = &-\sum_j log(q_j) - \int\beta\pi(\mathbf{r})d^3\mathbf{r} - \int\sum_m\rho_m(\mathbf{r})d^3\mathbf{r} \\
&-\frac{1}{2}\int\beta\langle\rho_q(\mathbf{r})\rangle\psi(\mathbf{r})d^3\mathbf{r} \\
&+\sum_a\sum_b\frac{\varepsilon_{ab}}{2}\int\int g_{ab}(|\mathbf{r}-\mathbf{r'}|)\langle\rho_a(r)\rangle\langle\rho_b(r)\rangle d^3\mathbf{r}d^3\mathbf{r'}
\end{aligned}
\tag{19}
$$

, where the index j runs over all grafting sites and m over all mobile species, which are H^+, OH^-, Na^+, Cl^- and water. Since the values of the free energy obtained through the above two methods were the same numerically in our calculations, we can conclude that the obtained density profiles were indeed the minimized profiles.

1.2 Molecular model

Polymer chains are generated using an iso-energetic three-state rotational isomeric state(RIS) model with a segment length of $\ell = 0.35$ nm.[4]. The conformations are generated using a simple sampling Monte Carlo method. All conformations are self-avoiding and do not penetrate the grafting surface. This was implemented in the chain generation by rejecting the entire chain as soon as overlap between any two monomers or a contact between the grafting surface and a monomer is noted and starting the whole process again. To obtain reliable average polymer-related quantities, we examined how our calculated density profiles varied with the number of conformations. We observed that beyond 0.5 million conformations, a further increase in the number conformations, did not produce any noticeable change in the obtained profiles. Notice that the above value also proved to be sufficient accurate in previous calculations of the Molecular Theory[3]. However, to completely eliminate the risk of numerical inaccuracies, a total of 1.5 million conformations (per graft point) were generated. To ensure that the set of conformations do not introduce any prior directional bias in the resulting microstructure in 3D calculations, these conformations included 12 30^o rotations of each randomly generated chain conformation following Tagliazucchi et. al.[3].

1.3 Biasing protocol for generation of microstructures under poor solvent conditions

As was emphasized in the main text, in 3D calculations, it is often challenging to obtain laterally inhomogeneous structures. Hence, one often resorts to biasing the system towards a microstructure of interest by choosing an initial guess for the algebraic equation solution having the symmetry of the expected microstructure. One such method of inducing a microstructure was developed by Huang and Szleifer[5]. Its underlying principle is to apply an external potential that satisfies the symmetry of the microstructure of interest. Solving the non-linear equations under this bias results in a solution conforming to the imposed symmetry. Then the bias is reduced gradually to zero, which is the equilibrium condition. If the symmetry of the biasing potential is appropriately selected, meaning it conforms with an intrinsic underlying physical "natural" symmetry of the system, then the non-biased equilibrium solution can correspond to a laterally inhomogeneous microstructure. Examples of it are shown in the main text. Mathematical details of this method are to be published in a separate work by the above authors in the future.

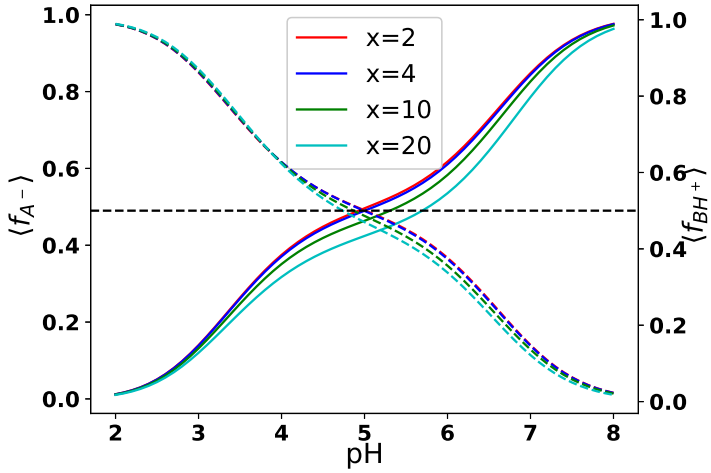

Fig. 1 Effect of blockiness on the dissociation behavior of A and B monomers. The total number of monomers of each species is 20 and the fraction of chargeable monomers for both A and B is 0.5. The copolymer is represented by $(A_xB_x)_n$, where x is the number of monomers in each block and n the number of blocks, meaning $xn = 20$. The salt concentration is 0.01 M.

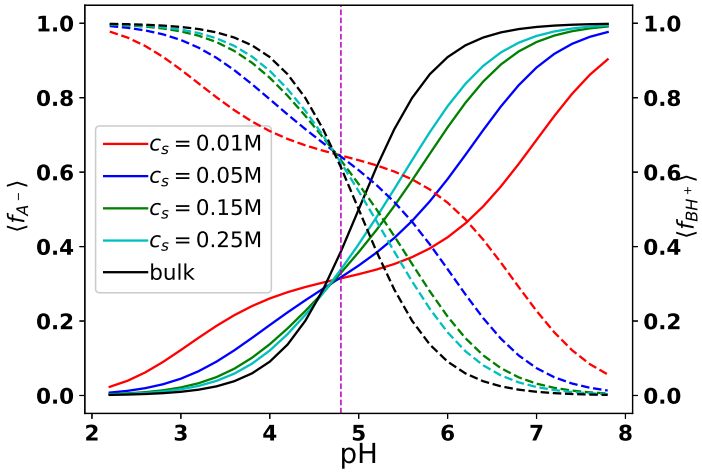

Fig. 2 The dissociation curves for $A_{20}B_{10}$ under various salt concentrations. The grafting density is 0.10 $nm^{-}2$.

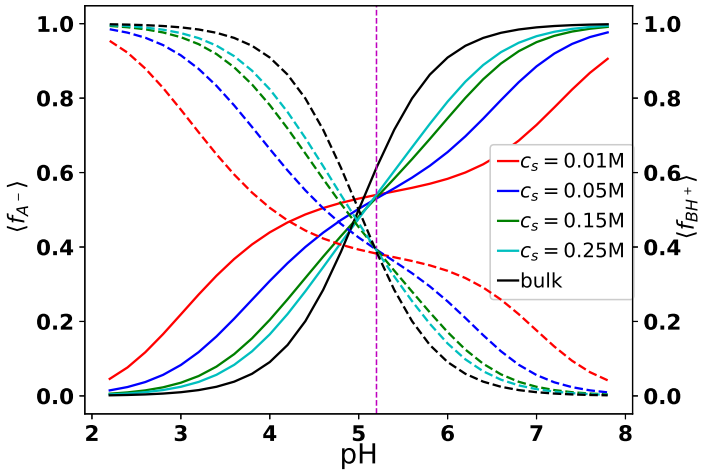

Fig. 3 The dissociation curves for $A_{20}B_{30}$ under various salt concentrations. The grafting density is 0.10 $nm^{-}2$.

2 Results

2.1 Effect of blockiness on the dissociation behavior of monomers

Figure 1 shows a comparison between polymers with different degrees of blockiness. It is seen that the degree of charging of the monomers is highest for alternating copolymers(x=2) and the least for the diblock copolymers(x=20). Since in the former, the oppositely charged monomers are already close to each other along the chain, the chain does not have to undergo any change in its conformation to decrease the electrostatic energy. However, as was explained in the main text, in the diblock copolymer, the conformational entropic cost of 'bending' the B block prevents all the oppositely charged monomers from coming close to each other, resulting in a decreased degree of charging.

2.2 Effect of asymmetry in chargeable monomer fraction

Here, we show the degree of charging as a function of pH for of different degrees of imbalance in the amount of acid and base monomers. Two asymmetric cases have been studied. Namely (a) $A_{20}B_{10}$ and (b) $A_{20}B_{30}$. In the first system, there is a surplus of acid monomers while in the second, base monomers are in the majority. Figures 2 and 3 depict the average degree of charging of both acid and base monomers for pH values 1 through 9, for $A_{20}B_{10}$ and $A_{20}B_{30}$, respectively. It is seen that when the amount of acid and base monomer is different, the symmetry of the charge curves around $pH = pK_a$ is broken. For an equal amount of acid base, the average degree of charge as function of pH is symmetric around $pH = pK_a$, as was observed in Figure 2 in the main text. When there are more acid monomers than base monomers, as in ($A_{20}B_{10}$), the isoelectric point, the pH for which the polymer has zero net charge, moves to the left. The reverse happens for the opposite case ($A_{20}B_{30}$). Please note that in these curves, the isoelectric point does not coincide with the pH marking the equality between acid and base charge fraction since the chargeable acid and base monomers in these systems are not equal in number. Rather the isoelectric point, pI, corresponds to value of the pH for which $\langle f_{A^-} \rangle N_A = \langle f_{BH^+} \rangle N_B$. More precisely, it is the pH of the cross-over from the upregulation to the downregulation of the acid monomer charge upon salt reduction in the direction of increasing pH. The same happens at pI for base monomers in the direction of decreasing pH. Hence, the isoelectric point is characterized by the pH at which the degree of dissociation is insensitive to the salt concentration. For $A_{20}B_{10}$ polymer, the deficit of B monomers means that for the net polymer charge to be zero, most B monomers must be charged and most A monomers uncharged. This happens when pH<pKa. The same reasoning also explains the rightward shift of the isoelectric point $A_{20}B_{30}$ case.

2.3 Effect of block length and sequence

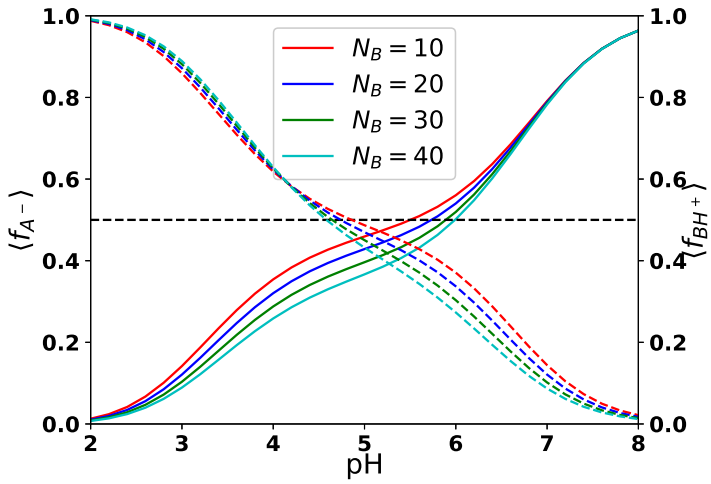

Fig. 4 Effect of the length of the B block on the dissociation behavior of A and B monomers for $A_{20}B_n$ block copolymers for different degree of polymerization of the B block. Here, the numbers of chargeable monomers on both block are the same and are equal to 10. This translates to a charge fraction of 0.5 for the A block. The corresponding value for the B block is adjusted accordingly. The salt concentration is $0.01M$. The grafting density corresponds to $\sigma_P = 0.10nm^{-2}$.

Figure 4 shows the effect of the length of the upper B block on the dissociation behavior of the A and B monomers. The figure presents the average degree of charge of the A and B monomers as a function of pH for different lengths of the upper B block. The A-blocks consist of $N_A = 20$ segments. The salt concentration is fixed at $c_S = 0.01M$. Other physical and chemical parameters, like the surface coverage, are the same for all cases.

Our aim here is to investigate the effect of polymer conformational entropy on the monomer dissociation behavior. Therefore, the total number of chargeable acid and base monomers is set to be equal. This means that with increasing length of the B-block, neutral B monomers are added to the polymer. We observe that with increasing block length, for the most part of the studied pH range, the average charge fraction of each block decreases. This is accompanied by a slightly enhanced asymmetric dissociation response of A and B monomers, i.e., the isoelectric point shifts away from pK_a towards higher pH values.

The electrostatic interactions and chemical equilibrium or the monomer dissociation, are coupled together. As argued above, oppositely charged acid and base monomers would prefer to be in each other's proximity. When the B block length N_B is small, the loss of entropy associated with "bringing" the B monomers closer to the A monomers is small and the gain in the attractive electrostatic energy outweighs the loss of conformational entropy. With increasing B-block length, the conformational entropic cost of bringing the A and B-block closer becomes more prohibitive. Thus, the electrostatic repulsion between like charges cannot be counterbalanced anymore by attractive electrostatic interaction between oppositely charged monomers that are placed close together. Instead, the system chemically alters the amount of charge to reduce the overall electrostatic repulsion between like-charged monomers, thus resulting in a decreased degree of charge of both monomers.

It is worth mentioning that at extremely low pHs, there is a slight increase in the degree of dissociation with increasing N_B. For low pH conditions, the A monomers are almost uncharged and B monomers are fully charged. Hence, electrostatic attraction between dissimilar monomers is almost absent irrespective of the value of N_B and the electrostatic repulsion between B monomers is the major contributor to the electrostatic energy. Increasing N_B while keeping the total number of charges constant spaces the chargeable B monomers further apart, hence reducing the energetic penalty to them being charged.

2.4 Homopolymer profile under different salt concentrations

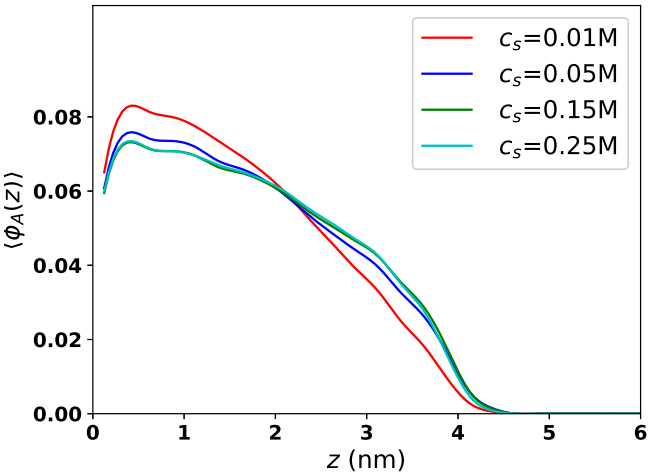

Fig. 5 The density profile of the A_{40} homo-polymer system at pH=6 at various salt concentrations. The grafting density is 0.10 nm^-2.

Fig. 5 gives A-monomer volume fraction profiles for (A_40) under various bulk salt concentrations. The corresponding pH is 6. It is seen that the monomer volume fraction profile does not change shape on salt removal and at low salt concentration, the brush contracts a little. This behavior is quite established in the literature [1,6] and we do not provide any further explanation here.

2.5 Proton concentration inside the brush at different pHs

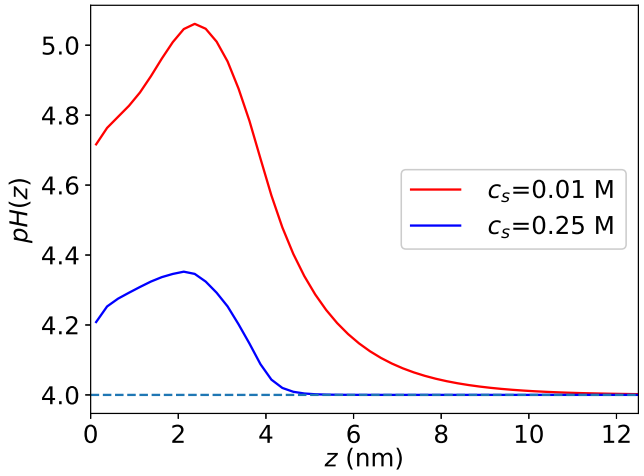

Fig. 6 Local pH ($-\log_{10}[H^+](z)$) inside the $A_{20}B_{20}$ brush as a function of distance under good solvent conditions at pH=4. The dashed line gives the bulk pH. The grafting density is 0.10 nm^{-2}.

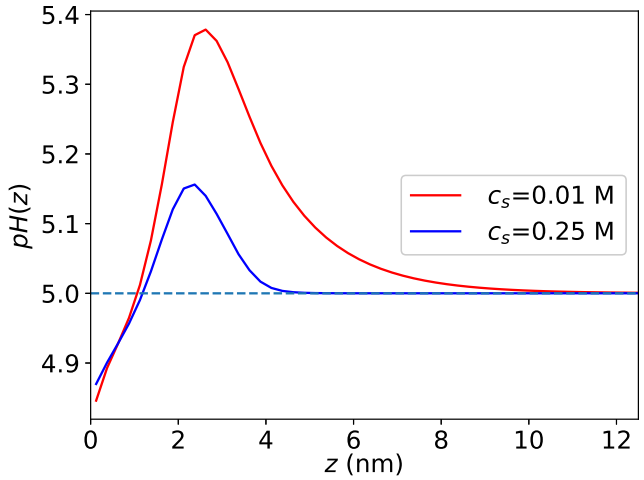

Fig. 7 Local pH ($-\log_{10}[H^+](z)$) inside the $A_{20}B_{20}$ brush as a function of distance under good solvent conditions at pH=5. The dashed line gives the bulk pH. The grafting density is 0.10 nm^{-2}.

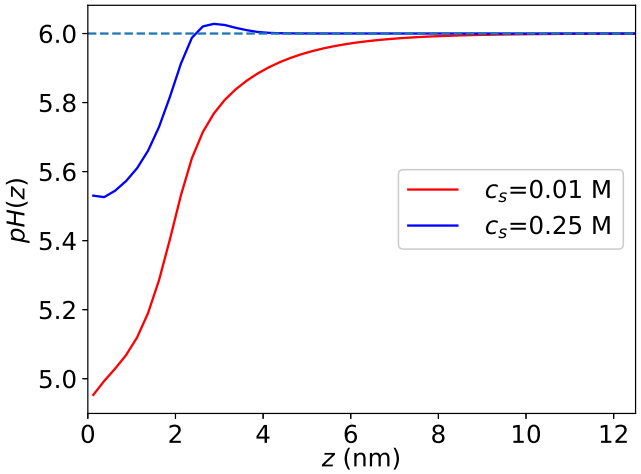

Fig. 8 Local pH ($-\log_{10}[H^+](z)$) inside the $A_{20}B_{20}$ brush as a function of distance under good solvent conditions at pH=6. The dashed line gives the bulk pH. The grafting density is 0.10 nm^{-2}.

2.6 Variation of height with pH at different salt concentrations

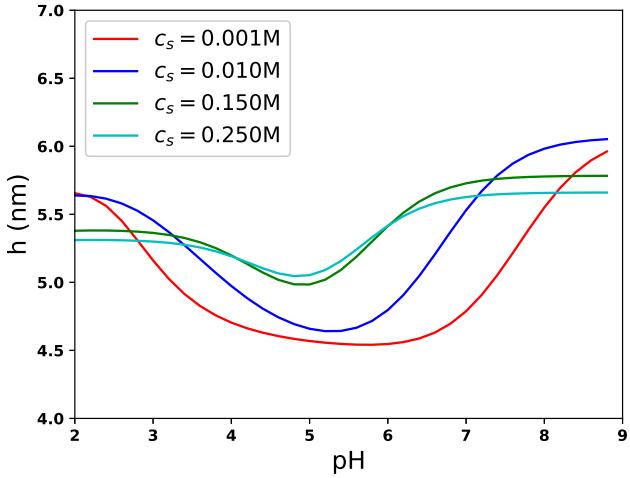

Fig. 9 The brush height as a function of pH at various salt concentrations. The grafting density corresponds to $\sigma_P = 0.10$ nm^{-2}. The fraction of chargeable monomers in each block is 0.5

2.7 Chemical potential vs grafting density under good solvent conditions

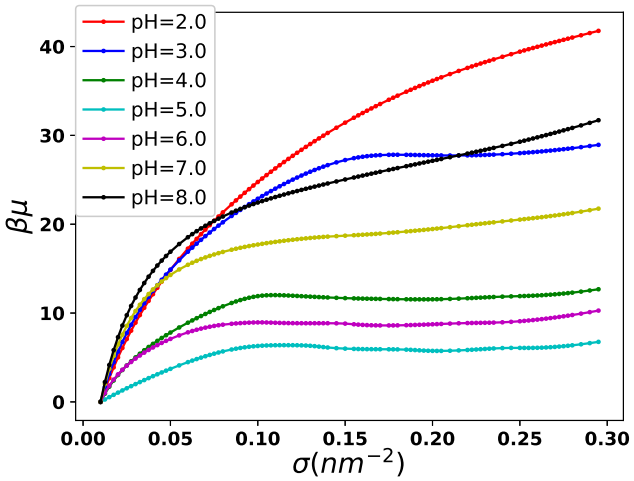

Fig. 10 Chemical potential of the polymer $A_{20}B_{20}$ as a function of surface coverage under good solvent conditions at various pH values. The salt concentration is 0.01 M. Here, 50 percent of both A and B monomers are dissociable.

Notes and references

1 R. Nap, P. Gong and I. Szleifer, *Journal of Polymer Science Part B: Polymer Physics*, 2006, **44**, 2638–2662.

2 A. C. Hindmarsh, P. N. Brown, K. E. Grant, S. L. Lee, R. Serban, D. E. Shumaker and C. S. Woodward, *ACM Transactions on Mathematical Software (TOMS)*, 2005, **31**, 363–396.

3 M. Tagliazucchi, M. O. de la Cruz and I. Szleifer, *Proceedings of the National Academy of Sciences*, 2010, **107**, 5300–5305.

4 P. Flory, *Macromolecules*, 1974, **7**, 381–392.

5 K. Huang and I. Szleifer, *APS*, 2018, **2018**, R28–010.

6 P. Gong, T. Wu, J. Genzer and I. Szleifer, *Macromolecules*, 2007, **40**, 8765–8773.